Inorganica Chimica Acta 470 (2018) 187–196

Contents lists available at ScienceDirect

Inorganica Chimica Acta

journal homepage: www.elsevier.com/locate/ica

Research paper

Synthesis, characterization, theoretical studies and biological activity of coordination compounds with essential metals containing N4-donor ligand 2,9-di(ethylaminomethyl)-1,10-phenanthroline

Luis Felipe Hernández-Ayala [a], Marcos Flores-Álamo [a], Sigfrido Escalante-Tovar [a], Rodrigo Galindo-Murillo [b], Juan Carlos García-Ramos [d,1], Jesús García-Valdés [c], Virginia Gómez-Vidales [d], Karen Reséndiz-Acevedo [a], Yanis Toledano-Magaña [a,1], Lena Ruiz-Azuara [a,*]

[a] Departamento de Química Inorgánica y Nuclear, Facultad de Química, Universidad Nacional Autónoma de México, Avenida Universidad 3000, 04510 Mexico City, Mexico
[b] Department of Medicinal Chemistry, College of Pharmacy, Skaggs Hall 201, University of Utah, Salt Lake City, UT 84112, United States
[c] Departamento de Química Analítica, Facultad de Química, Universidad Nacional Autónoma de México, Avenida Universidad 3000, 04510 Mexico City, Mexico
[d] Instituto de Química, Universidad Nacional Autónoma de México, Circuito Exterior s/n, Ciudad Universitaria, 04510 Mexico City, Mexico

ARTICLE INFO

Article history:
Received 1 March 2017
Received in revised form 12 June 2017
Accepted 14 June 2017
Available online 17 June 2017

Special Volume: Protagonists in Chemistry
Dedicated to Professor Carlo Mealli

Keywords:
1,10-Phenanthroline
Essential
Synthesis
Characterization

ABSTRACT

The work shows the synthesis and characterization of N4-donor **L**: 2,9-di(ethylaminomethyl)-1,10-phenanthroline and its coordination compounds with some divalent essential metals (Mn, Fe, Co, Ni Cu and Zn). **L** was obtained as the hydrochloride derivative H_3LCl_3. The complexes were synthesized by two routes: 1) using **L** as hydrochloride for Mn, Fe, Co and Zn complexes and 2) from **L** as a free base for Cu and Ni ones. $[Co(HL)Cl_2]NO_3$ and $[Zn(HL)Cl_2]Cl$ were crystallized and reveal that **L** is bound to metallic nuclei by only three nitrogen atoms. Cyclic voltammetry studies showed that **L** alone is capable of being reduced and in complexes, the potential of the coordinated compound process is lower. DFT calculations explain the observable redox behavior regarding HOMO-LUMO orbital energies. Also, the modeling of protonated species of the ligand **L** suggests that the tetradentate behavior depends on pH conditions of the synthesis. The antiproliferative activity observed on *Entamoeba Histolytica* and HeLa human tumor cell cultures confirmed that even if complexes are less active than the first choice drugs (metronidazole and cisplatin respectively), it exists a correlation between the observed cytotoxicity and the compounds redox potential.

1. Introduction

Most of the metal ions in the first transition row are essential trace elements for living beings. They are found in the active sites of many enzymes and are involved in several metabolic processes [1]. To regulate the amount of these elements within itself, the human body has different mechanisms (homeostatic processes), contrary to the other biological systems that do not have regulatory mechanisms and may present toxic effects when exposed to metallic compounds. The above, is one of the main factors that promote the chemists encourage their efforts to create and study coordination compounds with essential metals that help the mitigate diseases such as cancer [2–5], diabetes [6–8], parasitic diseases [9–12], among others.

A consequence of the planar nature of 1,10-phenanthroline is its ability to participate as a DNA intercalator [13], this same effect is observed in some of its metal complexes [14–16]. At the same time, some of this kind of complexes or natural products incorporating similar heterocyclic core possess interesting anticancer properties [17–19]. In particular, the coordination compounds of 2,9-di(ethylaminomethyl)-1,10-phenanthroline have shown great versatility in applications ranging from the recognition and catalysis of the hydrolysis in different molecules of biological interest [20–22] to the ability to interact with DNA [23]. These properties were used to design and to synthesize compounds with antitumor activity [24].

On the other hand, our group [25] revealed that coordination compounds with a nitrogen based hexadentate ligand, 2,9-bis (3,5-diazahexenyl)-1,10-phenanthroline and metals of the first

* Corresponding author.
E-mail address: lenar701@gmail.com (L. Ruiz-Azuara).
[1] At present: CONACYT-UNAM-Centro de Nanociencias y Nanotecnología-km 107 Carretera Tijuana-Ensenada, 22860 Ensenada, BC, Mexico.

http://dx.doi.org/10.1016/j.ica.2017.06.040
0020-1693/

transition series exhibit antitumor activity *in vitro* comparable to that shown by cis-Pt in human tumor cell lines CHP-212 (neuroblastoma) and HeLa (cervix). These compounds also presented unusual antiparasitic activity against *Entamoeba histolytica* cultures, some of them with a 100-fold potency greater than that observed for metronizadole.

The phenanthroline-based ligands and its coordination compounds own the ability to recognize and interact with biomolecules such as phosphates and DNA in a specific way. Besides, some of them possess redox and hydrolytic catalytic capacity. These properties could trigger different cellular mechanisms that produce the growth inhibition of several cultures such as tumor cells or protozoa.

In the present work, we reported the synthesis and characterization of 2,9-di(ethylaminomethyl)-1,10-phenanthroline trihydrochloride and their coordination compounds with essential metals. The structural characterization of all compounds carried out by different spectroscopic and analytical techniques, also, the X-ray crystal structures of $[Co(HL)Cl_2]NO_3$ and $[Zn(HL)Cl_2]Cl{\cdot}H_2O$ are presented. The redox behavior was analyzed by cyclic voltammetry and the electron density distribution through DFT calculations. Antiproliferative assays in tumor cells and amoebic cultures to investigate its potential biological activity are reported.

2. Experimental

2.1. Materials

2,9-dimethyl-1,10-phenanthroline (neocuproine) was purchased from (Sigma-Aldrich, Mexico) and used as received. 2,9-diformyl-1,10-phenanthroline was prepared according to the literature method [26–28]. Other reagents and solvents were RA quality. The solvents employed were dried by standard techniques before use.

2.2. Physicochemical measurements

A Fisons Instruments analyzer model EA 1108 was used for elemental analysis determination, using a sulfanilamide standard. Nicolet Avatar 320 FT-IR spectrometer was used to record the infrared spectra from the KBr pellet in the region of 400–4000 cm^{-1}. Mass spectra were obtained with a JEOL SX102A mass spectrometer with a matrix of nitrobenzyl alcohol; the samples were dissolved in CH_3OH. A VARIAN Unity Inova spectrometer was used to record all NMR spectra, 1H (300 MHz) and 13C (75.5 MHz); TMS was the reference and D_2O to dissolve compounds H_3LCl_3 and $[Zn(HL)Cl_2]Cl{\cdot}H_2O$ A dual beam spectrophotometer (ThermoFisher Scientific, Genesys 10S) was used to acquire UV–vis spectra in the range of 200–1200 nm using DMSO as a solvent. The solid diffuse reflectance spectra were acquired (Agilent, Cary 5000 UV–Vis-NIR spectrophotometer) in the range of 175–33000 cm^{-1}. The EPR spectra were obtained in DMSO solution (Jeol, TES-300 spectrophotometer) operating at the X-band, at a modulation frequency of 100 kHz and a cylindrical cavity in the mode TE_{011} and were measured at T = −195.8 °C. Magnetic susceptibility data were collected with a Magnetic Susceptibility Balance (Sherwood Scientific, MK-1). The conductivity data were obtained at sample concentrations of ca. 1×10^{-3} M in DMSO solutions at 25.0 °C (JENWAY 4330 conductivity-pH meter). All electrochemical measurements were performed in DMSO (HPLC grade) using an EDAQ EA161 or PAR 273A potentiostats/galvanostats, both controlled by PC software. X-ray diffraction measurements were acquired on an Oxford Diffraction Gemini-Atlas diffractometer.

2.3. Synthesis of 2,9-di(ethylaminomethyl)-1,10-phenanthroline trihydrochloride (H_3LCl_3)

2,9-Diformyl-1,10-phenanthroline (2 mmol, 0.54 g) was suspended in 50 ml of dry EtOH, and 4 mmol of ethylamine (0.120 ml) was added, the formed solution was kept under reflux and stirred for 4 h. Solid $NaBH_4$ (8 mmol, 0.30 g) was added to the reaction mixture in small portions. The above solution had been stirred for 12 h, and it was concentrated until a pale yellow solid appeared. The residue was dissolved in 25 ml water and extracted three times with 15 ml $CHCl_3$. The organic extract was concentrated to yield a yellow oil. The oil was dissolved in 5 ml EtOH and conc. hydrochloric acid was added (2 mmol, 0.165 ml). The resulting yellow solid was filtered and washed with a small portion of EtOH. Final recrystallization of the product was carried out from MeOH and filtered through an activated charcoal bed resulting in a white powder.

H_3LCl_3 *white powder:* Yield (75%); Anal. Calc. $H_3C_{18}H_{22}N_4Cl_3{\cdot}2H_2O$, (439.81 g/mol): C(49.38), H(6.21), N(12.79). Found: C (49.42), H(6.45), N(12.70)%. NMR ^1H (for reference about NMR assignation see Fig. S1): δ = 1.29 (t, 3H, CH_3-, J = 5.1 Hz), 3.19 (q, 2H, CH_3-CH_2- J = 5.4 Hz), 4.51 (s, 2H, -CH_2-Phen), 7.50 (s, 1H, Phen H-$C_{7,8}$), 7.58 (d, 1H, Phen H-$C_{5,12}$, J = 6.3 Hz), 8.14 (d, 1H, Phen H-$C_{11,6}$, J = 6.3 Hz). NMR ^{13}C): δ = 10.63 (CH_3-), 43.05 (CH_3-CH_2-), 51.10 (NH-CH_2-Phen), 122.95 (Phen $C_{7,8}$), 126.66 (Phen $C_{5,12}$), 128.38 (Phen $C_{1,9}$), 138.52 (Phen $C_{6,11}$), 143.45 (Phen $C_{4,13}$), 151.11 (Phen $C_{2,10}$). MS: m/z (%) 295 (100)$[HL]^+$, 331 (10) $[H_2LCl]^+$; IR, (KBr): ν = 3419, 2946, 2788, 1631, 1610, 1542, 1457, 1436, 1351, 881 cm^{-1}. UV–Vis (DMSO): λ_{max} (ε), nm ($M^{-1}\,cm^{-1}$); 326 (869), 276 (22559). UV–vis (DR): no bands appear (limit 250 nm). Λ(DMSO)(μS): 53.8. $E_{1/2}$ (V vs Fc^+/Fc): −0.793 ($L + e^- \rightarrow L^-$).

2.4. Synthesis of coordination compounds of L

The coordination compounds were synthetized by two different routes:

Method 1) A solution with 1 mmol (0.440 g) of H_3LCl_3 in 10 ml of water was added to another with 1 mmol of the corresponding metal salt ($MnCl_2{\cdot}4H_2O$, $Co(NO_3)_2{\cdot}6H_2O$, $FeCl_2{\cdot}4H_2O$, and $ZnCl_2{\cdot}4H_2O$) in the same amount of solvent. The resultant solution was adjusted to pH = 6 by additions of NaOH 0.1 M. After 2 h of stirring at room temperature, solvent was evaporated slowly at vacuum. To precipitate the iron compound 1 mmol (0.340 g) of solid ammonium tetraphenylborate was added.

$[Mn(HL)Cl]Cl_2$ *Orange needles:* Yield (81%); Anal. Calc. $[Mn(HC_{18}H_{22}N_4)Cl]Cl_2{\cdot}2H_2O$, (492.72 g/mol): C(43.9), H(5.5), N(11.4). Found: C(44.0), H(5.7), N(10.9)%. MS: m/z (%) 384 (100) $[Mn(L)Cl]^+$, 420 (10) $[Mn(HL)Cl_2]^+$; IR, (KBr): ν = 3446, 2977, 2939, 2792, 1621, 1591, 1565, 1454, 1430, 1377, 866 cm^{-1}. UV–Vis(DMSO): λ_{max} (ε), nm ($M^{-1}\,cm^{-1}$); 493 (197), 443 (226), 440(s), 326 (1790), 279 (22390). UV–Vis (DR), nm: 349, 442, 472, 504 Λ (DMSO) (μS): 52.9. μ_{eff} (BM): 5.62; EPR (DMSO, −198.5 °C): g = 2.0085, A = 82.79×10^{-4} cm^{-1}. $E_{1/2}$ (V vs Fc^+/Fc): E_{pc} = −1.341 ($Mn^{II}L + e^- \rightarrow Mn^{II}L^-$), $E_{1/2}$ = −1.942 ($Mn^{II}L^- + e^- \rightarrow Mn^{II}L^{2-}$).

$[Fe(HL)Cl_2]B(Ph)_4$ brown powder: Yield: 71%. Anal. Calc. $[Fe(HC_{18}H_{22}N_4)Cl_2]B(C_6H_5)_4{\cdot}H_2O$, (759.39 g/mol): C(66.4), H(6.0), N (7.4). Found: C(66.6), H(6.1), N(7.5)%. MS: m/z (%) 385 (10) $[Fe(HL)Cl]^+$, 136 (100) $[(CH_3)_2$-Ph-$(NH_4)]^+$. IR, (KBr): ν = 3475, 3218, 3051, 2983, 2788, 1579, 1504, 1475, 1430, 1374, 860, 737, 706 cm^{-1}. UV–Vis (DMSO): λ_{max} (ε), nm ($M^{-1}\,cm^{-1}$); 320 (s), 281 (20855). UV–Vis (DR), nm: 411. Λ (DMSO)(μS): 35.4. μ_{eff} (BM) = 3.67. $E_{1/2}$ (V vs Fc^+/Fc): −1.055 ($Fe^{II}L + e^- \rightarrow Fe^{II}L^-$), $E_{1/2}$ = −1.272 ($Fe^{II}L^- + e^- \rightarrow Fe^{II}L^{2-}$), E_{pa} = +0.442 ($Fe^{II}L \rightarrow Fe^{III}L + e^-$).

[Co(HL)Cl$_2$]NO$_3$ *Orange needles:* Yield (85%). Anal. Calc. [Co($HC_{18}H_{22}N_4$)Cl_2]NO_3·H_2O (487.24 g/mol): C(44.0), H(5.1), N(11.4). Found: C(44.4), H(4.8), N(11.8)%. MS: *m/z* (%) 388 (100) [Co(L)Cl]$^+$, 424 (70) [Co(HL)Cl_2]$^+$. IR, (KBr): ν = 3479, 3185, 2967, 2941, 2790, 1619, 1571, 1448, 1429, 1382, 867 cm^{-1}. UV–Vis (DMSO): λ_{max} (ε), nm (M^{-1} cm^{-1}); 676 (70), 612 (77), 548 (55), 276 (22407), 296 (s). UV–vis (DR), nm: 542, 600, 1200 Λ (DMSO) (μS): 31.3. μ_{eff} (BM): 2.07. EPR (solid, −198.5 °C): g = 2.29. $E_{1/2}$ (V vs Fc$^+$/Fc) = −1.471 ($Co^{II}L + e^- \rightarrow Co^{II}L^-$), $E_{1/2}$ = −1.645 ($Co^{II}L^- + e^- \rightarrow Co^{II}L^{2-}$), $E_{1/2}$ = +0.226 ($Co^{III}L + e^- \rightarrow Co^{II}L$). Suitable crystals were obtained by recrystallization with MeCN/water 10:1 mixture.

[Zn(HL)Cl$_2$]Cl *White needles:* Yield (82%); Anal. Calc. [Zn($HC_{18}H_{22}N_4$)Cl_2]Cl·$5H_2O$, (520.78 g/mol): C(41.5), H(6.2), N (10.7). Found: C(41.8), H(6.3), N(10.8)%. NMR ^{1}H (for reference about NMR assignation see Fig. S1): δ = 1.27 (t, 3H, CH_3-, *J* = 5.4 Hz), 3.10 (q, 2H, CH_3-CH_2- *J* = 5.4 Hz), 4.50 (s, 2H, -CH_2-Phen), 7.58 (s, 1H, Phen H-$C_{7,8}$), 7.75 (d, 1H, Phen H-$C_{5,12}$, *J* = 6.3 Hz), 8.34 (d, 1H, Phen H-$C_{6,11}$, *J* = 6.6 Hz). NMR ^{13}C: δ = 12.44 (CH_3-), 44.48 (CH_3-CH_2-), 51.05 (NH-CH_2-Phen), 124.91 (Phen $C_{7,8}$), 126.88 (Phen $C_{5,12}$), 128.38 (Phen $C_{1,9}$), 139.46. (Phen $C_{4.13}$), 140.95 (Phen $C_{6,11}$), 154.93 (Phen $C_{2,10}$). MS: *m/z* (%) 431 (100) [Zn(HL)Cl_2]Cl$^+$, 395 (90) [Zn(HL)Cl_2]$^+$. IR, (KBr): ν = 3407, 2969, 2935, 2792, 1619, 1592, 1569, 1467, 1423, 1382, 864 cm^{-1}. UV–Vis (DMSO): λ_{max} (ε), nm (M^{-1} cm^{-1}); 327(s), 300(s), 278 (21719). UV–vis (DR): No bands appear; Λ (DMSO) (μS): 37.5. E_{pc} (V vs Fc$^+$|Fc): −1.514 ($Zn^{II}L + e^- \rightarrow Zn^{II}L^-$), $E_{1/2}$ = −1.882 ($Zn^{II}L^- + e^- \rightarrow Zn^{II}L^{2-}$). Suitable crystals were obtained by recrystallization with MeCN/water 10:1 mixture.

Method 2) 3.3 mmol of solid NaOH (0.130 g) was added to an aqueous solution (10 mL) containing 1.1 mmol of H_3LCl_3 (0.485 g), after 0.5 h of strong stirring, the free base L was extracted with CH_2Cl_2 (3 × 10 mL). The organic extracts were mixed and the solvent was evaporated. The oily residue was dissolved in 10 ml of MeCN. This solution was added to another previously prepared containing 1 mmol of the metallic salt $Cu(NO_3)_2$·$2.5H_2O$ and Ni $(NO_3)_2$·$6H_2O$) in 10 ml of the same solvent. After two hours of stirring, powders of different shades of green begin to precipitate. The powders were washed three times with cold MeCN.

[Cu(L)(H$_2$O)](NO$_3$)$_2$ *dark green needles*: Yield (50%); Anal. Calc. [Cu($C_{18}H_{22}N_4$)(H_2O)](NO_3)$_2$, (499.96 g/mol): C(43.2), H(4.8), N (16.4); Found: C(43.7), H(4.5), N(16.8)%. MS: *m/z* (%) 357 (100) [Cu(H_{-1}L)]$^+$, 419 (33) [Cu(L)NO_3]$^+$. IR, (KBr): ν = 3421, 3207, 2973, 2937, 1623, 1592, 1581, 1506, 1467, 1384, 868 cm^{-1}. UV–Vis (DMSO): λ_{max} (ε), nm (M^{-1} cm^{-1}); 455 (326), 281 (22727). UV–Vis (DR), nm: 733, 1383. Λ (DMSO) (μS): 88.0. μ_{eff} (BM): 1.98. EPR (DMSO, −198.5 °C): g = 2.064, $g_{||}$ = 2.27, $A_{||}$ = 150 × 10^{-4} cm^{-1}, A = 14.48 × 10^{-4} cm^{-1}. E_{pa} (V vs Fc$^+$/Fc): −1.310 ($Cu^{II}L + e^- \rightarrow Cu^{II}L^-$), $E_{1/2}$ = −0.348 ($Cu^{II}L + e^- \rightarrow Cu^{I}L$), E_{pc} = −0.722 ($Cu^{I}L + e^- \rightarrow Cu^0 + L$).

[Ni(L)(H$_2$O)(NO$_3$)]NO$_3$ *pale green powder:* Yield (64%). Anal. Calc. [Ni($C_{18}H_{22}N_4$)(H_2O)(NO_3)]NO_3·H_2O, (513.12 g/mol): C(42.1), H (5.1), N(16.4). Found: C(42.4), H(4.6), N(16.1)%. MS: *m/z* (%) 414 (20)[Ni(L)NO_3]$^+$, 351 (100) [Ni(H_{-1}L)]$^+$. IR, (KBr): ν = 3299, 3228, 2971, 1623, 1592, 1573, 1504, 1467, 1390, 1384, 867 cm^{-1}. UV–Vis (DMSO): λ_{max} (ε), nm (M^{-1} cm^{-1}): 350 (368) 305 (s), 279 (23104). UV–vis (DR): 612, 836, 1044 nm. Λ (DMSO) (μS): 74.6. μ_{eff} (BM): 2.86. E_{pc} (V vs Fc$^+$/Fc): −1.110 ($Ni^{II}L + e^- \rightarrow Ni^{II}L^-$), $E_{1/2}$ = −1.782 ($Ni^{II}L^- + e^- \rightarrow Ni^{II}L^{2-}$).

2.5. Electrochemical studies

Electrochemical measurements were performed at sample concentrations of 2 × 10^{-3} M in DMSO solution containing 0.1 M of $TBAPF_6$ (Tetra-N-butylammonium hexafluorophospate). The potentiostats/galvanostats (EDAQ EA161 or PAR 273A) were used with the typical three-electrode array. A platinum disk (ϕ = 1 mm) was used as working electrode. A platinum wire served as a counter-electrode, and a silver wire was used as a pseudo-reference electrode. Prior each measurement, the solutions were bubbled with nitrogen. The electrochemical behavior was explored using cyclic voltammetry initiated from open circuit potential. All measurements were recorded using a scan rate of 100 mV s^{-1}. Potentials were reported versus the couple Fc-Fc$^+$ according to IUPAC [29]. The current interrupt method was used for ohmic (iR) compensation in all the experiments.

2.6. X-ray crystal structure determination

Single crystals of [Co(HL)Cl_2]NO_3 or [Zn(HL)Cl_2]Cl·H_2O compounds were mounted on glass fibre to be studied with the diffractometer, equipped with a CCD area detector, a sealed tube X-ray source ($\lambda_{MoK\alpha}$ = 0.71073 Å) and a monochromator of graphite. The method of scanning was the double pass to avoid noise. Collected frames were integrated using an orientation matrix determined from the narrow frame scans. CrysAlis Pro and CrysAlis RED software packages [30] were employed to collect and integrate data. Integrated data analysis did not reveal any decay. Final cell parameters were determined by a global refinement of reflections. Collected data were rectified for absorbance by analytical numeric absorption correction [31], using a multifaceted crystal model based on expressions upon the Laue symmetry using equivalent reflections.

Structure solution and refinement were carried with the programs SHELXS-2014 and SHELXL-2014 respectively [32]; for molecular graphics: ORTEP-3 for Windows [33]; and the software used to prepare material for publication: WinGX [34]. Full-matrix least-squares refinement was carried out by minimizing $(Fo^2 - Fc^2)^2$. All non-hydrogen atoms were refined anisotropically.

For H atom of the water group (H—O) and amine group (H-N) were located in a difference map and refined isotropically with Uiso(H) = 1.5 for H—O, and Uiso(H) = 1.2 for H—N. H atoms attached to C atoms were placed in geometrically idealized positions and refined as riding on their parent atoms, with C—H = 0.95 and 0.99 Å with U_{iso} (H) of 1.2U_{eq}(C) for methylene and aromatic groups and 1.5U_{eq}(C) methyl groups. Crystal data and experimental details of the structure determinations are listed in Table 1.

Crystallographic data have been deposited at the Cambridge Crystallographic Data Center as supplementary material number CCDC 1535013–1535014. Copies of the data could be obtained free of charge on application to CCDC, 12 Union Road, Cambridge CB2 1EZ, UK. E-mail: deposit@ccdc.cam.ac.uk.

2.7. Computational details

Electronic properties and calculations of all the complexes were calculated using Gaussian 09 (ver. D01) [35] using the M06-2X [36,37] level of theory with a 6-31G(d,p) basis set. The ligand and [Zn(L)Cl_2]·H_2O calculations were performed using the Kohn-Sham formalism as implemented in deMon2k [38], version 4.3.4. The basis set was DZVP [39] with the PBE [40] exchange-correlation functional. Harmonic frequency calculations were performed to obtain the corresponding thermochemical corrections and to confirm that the structures obtained correspond to a minimum energy structure. A full geometric optimization, starting from the available crystallographic structures, was performed for each transition metal complex presented on this work. The DFT functional employed has been proven in previous work to successfully represent the type of compounds studied here [41–43]. For each optimization, frequency analysis showed no negative results, ensuring full structural convergence. All calculations were performed in the gas phase.

Table 1
Crystal data and structure refinement for $[Co(HL)Cl_2]NO_3$ and $[Zn(HL)Cl_2]Cl{\cdot}H_2O$.

Identification code	$[Co(HL)Cl_2]NO_3$	$[Zn(HL)Cl_2]Cl{\cdot}H_2O$
Empirical formula	C18 H23 Cl2 Co N5 O3	C18 H25 Cl3 N4 O Zn
Formula weight	487.24	485.14
Temperature	130(2) K	130(2) K
Wavelength	0.71073 Å	0.71073 Å
Crystal system	Monoclinic	Monoclinic
Space group	P 21/c	C 2/c
Unit cell dimensions	a = 16.4250(9) Å b = 8.8552(4) Å c = 14.9998(7) Å β = 103.809(5)°.	a = 28.658(2) Å b = 10.8432(9) Å c = 13.4876(9) Å β = 99.694(7)°.
Volume	2118.61(19) $Å^3$	4131.4(5) $Å^3$
-Z	4	8
Density (calculated)	1.528 Mg/m^3	1.560 Mg/m^3
Absorption coefficient	1.092 mm^{-1}	1.593 mm^{-1}
F(000)	1004	2000
Crystal size	0.483 × 0.330 × 0.161 mm^3	0.580 × 0.140 × 0.080 mm^3
Theta range for data collection	3.438–29.443°	3.564–29.537°
Index ranges	$-20 \le h \le 21$, $-11 \le k \le 12$, $-19 \le l \le 20$	$-32 \le h \le 38$, $-13 \le k \le 14$, $-16 \le l \le 17$
Reflections collected	14609	11851
Independent reflections	5070 [R(int) = 0.0489]	4963 [R(int) = 0.0434]
Completeness to theta = 25.242°	99.7%	99.7%
Refinement method	Full-matrix least-squares on F^2	Full-matrix least-squares on F^2
Data/restraints/parameters	5070/3/273	4963/5/261
Goodness-of-fit on F^2	1.064	1.060
Final R indices [I > 2sigma(I)]	R1 = 0.0465, w*R2* = 0.0850	R1 = 0.0444, w*R2* = 0.0702
R indices (all data)	R1 = 0.0859, w*R2* = 0.1051	R1 = 0.0797, w*R2* = 0.0851
Largest diff. peak and hole	0.407 and −0.445 e $Å^{-3}$	0.426 and −0.501 e $Å^{-3}$

2.8. Antiproliferative activity assays

2.8.1. Parasite culture and amoebicidal activity

Entamoeba histolytica HM1: IMSS trophozoites were axenically grown in TYI-S33 medium. Trophozoites (1×10^5) were placed in tubes with 3 ml of TYI-S33 medium supplemented with Adult Bovine Serum (10%), Diamond vitamins (5%) and antibiotic (1%) incubating at 37 °C and 5% CO_2. Each compound was added to reach the final concentrations as follows: 1000, 100, 10, 1, 0.1 and 0.01 μM. Amoebic trophozoites viability was assessed employing optical microscope with vital marker trypan blue and confirmed with fluorescent staining with carboxyfluorescein diacetate (CFDA) and propidium iodide (PI) as markers. Trophozoite viability determinations were done at 24, 48 and 72 h. In brief, 100 μl samples containing around 1×10^4 treated parasites were added with trypan blue (5 μL, 0.4%) or CFDA (1 μL) or PI (1 μL). Cell viability was determined with an hemocytometer in an optical or fluorescent microscope.

2.8.2. Human tumor cell culture and antiproliferative activity

2×10^4 HeLa cells (ATCC) per well were plated in a 96-well microplate (Costar®) with Dulbecco's modified Eagle medium (D-MEM) supplemented with 10% fetal bovine serum (FBS) and allowed to attach incubating at 37 °C and CO_2 (5%) for 24 h. At the end of incubation time, the medium was aspirated, and cells were exposed to 10 μL of test solution at different concentrations (1, 3, 10, 30, 100 and 300 μM) for 24 h under the conditions mentioned above. Cell growth was determined according to the sulforhodamine B assay [44,45]. Absorbance was measured at 564 nm in a Microplate reader BIORAD 550 and percentage of cell growth at each concentration of drug was calculated as growth% = 100 × [T/C], where T is the absorbance of treated wells and C is the absorbance of untreated wells. This equation was used to determine the concentration needed to inhibit the culture growth in a 50%. Reported IC_{50} values are the average of at least three independent experiments. Details of measuring cell growth inhibition are described elsewhere [44].

3. Results and discussion

3.1. Synthesis and structural characterization of L and its coordination compounds with essential metals ions

The ligand L was synthesized through the route outlined in Fig. 1. Since it is an oily product, we purify it by precipitation adding conc. HCl to get the hydrochloride salt. The elemental analysis showed this salt was L in its trihydrochloride form. In DMSO solution, H_3LCl_3 is partially dissociated, and it behaves like a 1:1 electrolyte ($H_3LCl_2^+$ Cl^-) according to the measured conductivity value (53.8 μS).

Initially, we tried to prepare $[M(L)]^{2+}$, in aqueous media, by the reaction of MX_2 (X = Cl^-, NO_3^-) with an equimolar amount of H_3LCl_3 and adjusting the solution pH by adding NaOH as described by H. Sun and coworkers [46]. Although this method was satisfactory for manganese, cobalt and zinc complexes, products precipitated as needles, resulted unsatisfactory for the iron, copper and nickel ones since products obtained were oils. To overcome this obstacle, we change the counter-ion in the iron complex while the copper and nickel compounds were synthesized using MeCN as a solvent and L in its free base form.

Structures of Co(II)L and Zn(II)L complexes were unambiguously established by single crystal X-ray diffraction analysis. Structures of Mn(II), Fe(II), Ni(II) and Cu(II) were proposed through elemental analysis, IR, EPR, UV–vis, mass spectrometry, conductivity and magnetic susceptibility measurements. The IR spectroscopy showed that the bands, associated with the vibration of the aromatic C=N (1506 and 1610 cm^{-1}) and aliphatic C-N (3200 cm^{-1}) bonds of L, after coordinating the metal ion shifted at high frequencies. Also, a robust band of L close to 2788 cm^{-1}, assigned to aliphatic protonated amine ν(N+-H), was slightly shifted to higher frequencies due to coordination and only appears in Mn(II), Fe(II), Co(II) and Zn(II) complexes. That fact infers L is protonated in these compounds and agrees with the results obtained from X-ray diffraction analysis (see below).

The signal assignation of NMR ^1H spectra for Zn(II) complex acquired in D_2O, was done by direct comparison with those signals

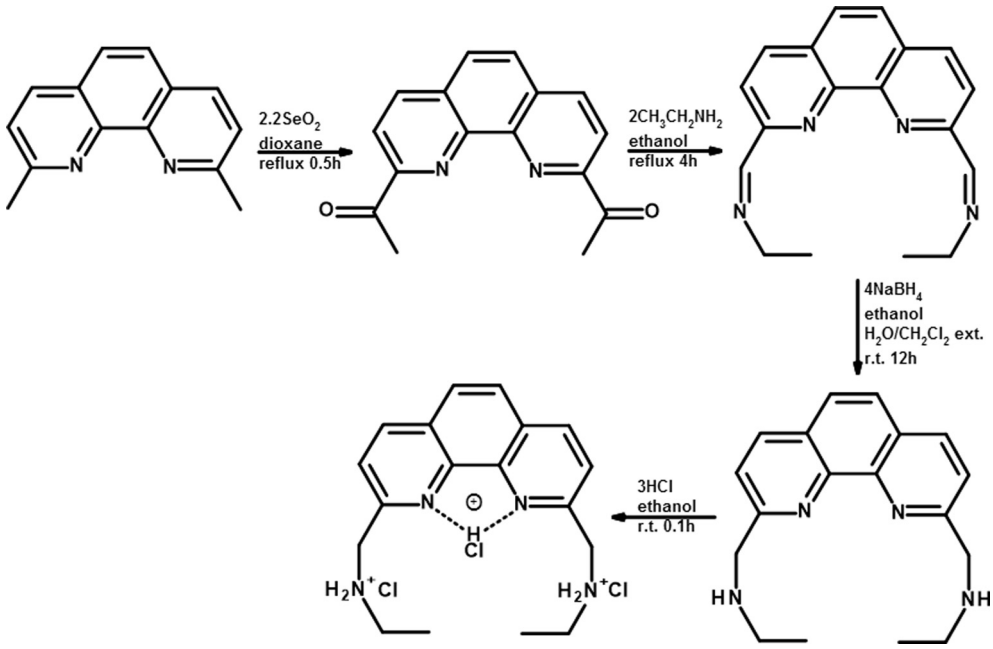

Fig. 1. Synthesis of ligand hydrochloride, H_3LCl_3. (2 columns).

identified in the spectra of the protonated ligand H_3LCl_3 (Figs. S1, S2 and Table S1). The protons of the 1,10-phenanthroline moiety of the ligand and their corresponding signals in the coordination compound were observed between 7.50 and 8.40 ppm. A small shift (0.1–0.2 ppm) to lower field in these signals was observed due to the coordination to the metal ion. Also, a slight displacement to high field, compared with those found for L, is observed for the signals associated with the hydrogen atoms attached to the aliphatic nitrogen atoms of Zn(II) complex. This fact suggests that in D_2O solution, the ligand can bind strongly to Zn via aromatic nitrogen atoms, but the bond with the nitrogen of the secondary amines is weak. That information indicates a transition between the four-coordinated distorted tetrahedral to distorted octahedral geometry passing by a penta-coordination due to the weak aliphatic nitrogen coordination described above.

$[Mn(HL)Cl]Cl_2$ EPR spectra, in DMSO frozen solution at −198 °C, exhibit a pseudoisotropical signal centered at g = 2.0085, with six hyperfine lines as expected for $^{55}Mn(II)$ complex, due the central transition (+1/2 → −1/2) with a hyperfine coupling constant $A = 82.79 \times 10^{-4}\ cm^{-1}$. The EPR data and the 5.62 BM of μ_{eff} are in agreement with an S = 5/2 Mn(II) center [47]. Three bands observed in both electronic spectra, solid state, in DMSO solution and electrolytic conductivity of 52.9 μS suggest a tetrahedral geometry with three nitrogen atoms from L and a chlorido linked directly to the Mn(II) center to get $[Mn(HL)Cl]Cl_2$. In the case of $[Fe(HL)Cl_2]B(Ph)_4$ complex, the μ_{eff} = 3.67 BM and Λ = 35.4 μS (DMSO) indicate a penta-coordination with a trigonal bipyramid arrangement around the metal. Cu(II), and Ni(II) compounds give the same type of information, so the same conformation is proposed. The $\nu(N^+\text{-}H)$ signal, in these complexes, was not observed indicating that L is totally deprotonated. The shape and values of EPR signals for $[Cu(L)(H_2O)](NO_3)_2$ ($g^{\perp} = 2.069$, $g_{\parallel} = 2.27$, $A_{\parallel} = 150 \times 10^{-4}\ cm^{-1}$, $A^{\perp} = 14.48\ cm^{-1}$, S = 1/2) let us to consider an axial spectrum that corresponds to a square-base pyramidal geometry in solid state and, with a coordination of a solvent molecule, octahedral in frozen DMSO solution, respectively. The $[Ni(L)(H_2O)(NO_3)]NO_3$ IR spectrum showed a double band in the region of 1380–1390 cm^{-1} which is indicative of two types of nitrate ion [48], the first one linked directly to the metal and the second one as a counter ion. The above fact, the three bands in UV–vis-NIR spectrum (acquired in the solid state) and the μ_{eff} measurement, are indicative of an octahedral geometry in the solid state for the Ni(II) complex. In DMSO solution, the information was insufficient to conclude about the geometry.

After acetonitrile-water recrystallization, analysis of single crystals by XRD revealed that $[Co(HL)Cl_2]NO_3$ and $[Zn(HL)Cl_2]Cl$ crystallize in the monoclinic space groups *P*21/*c* and *C*2/*c* respectively. Table 1 summarizes crystals data collection and the refinement parameters. Selected bond lengths and angles are listed in Table 2. An ORTEP diagram of cationic part of the complexes is shown in Fig. 2. In the cobalt complex the anion is nitrate, and for the zinc one is chloride. In both cases, the metal ion shows a five-coordinated bonding by three nitrogen atoms of the ligand L and two chloride ions. They show rather unsaturated coordination spheres. In penta-coordinated compounds, the angular distortion value τ [49], is a key parameter to describe the geometry. Since the Co(II) and the Z(II) complexes have τ values of 0.61 and 0.52, respectively, their geometry is an intermediate between square pyramidal and trigonal bipyramid. Cobalt shows short (2.01 and 2.07 Å) and zinc long (2.36–2.39 Å) M—N bond lengths with the aromatic nitrogen. The bond length of metal-aliphatic nitrogen is quite similar in both cases (Co = 2.167 Å and Zn = 2.172 Å) both bond lengths indicate that the metal is not centered on L. On the other hand, the uncoordinated nitrogen atom (N3) of the aliphatic residue from L is protonated. One of the hydrogen atoms linked to N3 participates in an intramolecular hydrogen bond with a coordinated chloride, N-H···Cl = 2.23(1) Å. In the crystal array, there are intermolecular hydrogen bond interactions of the type N-H···O and N-H···Cl. Especially for the cationic complex $[Co(HL)Cl_2]^+$, the N3-H3E···O1 and N3-H3E···O2 produce an $R_2^1(4)$ motif. Similar interactions were observed in the Zn(II) compound, where the hydrogen bond interactions O1w-H1D···Cl1 and O1W-H1E···Cl3 show the $D_2^2(5)$ motif.

Finally, notice that the ligand rigidity, imposed by the large heteroaromatic moiety, does not allow the simultaneous coordination of both aliphatic nitrogen atoms and the heteroaromatic ones to the same metal ion. At least in this geometry, in axial

Table 2
Selected bond lengths (Å) and angles (°) for $[Co(HL)Cl_2]NO_3$ and $[Zn(HL)Cl_2]Cl$.

$[Co(HL)Cl_2]^+$				$[Zn(HL)Cl_2]^+$			
Bond Lengths (Å)							
Co-N1	2.362(2)	Co-Cl1	2.2512(9)	Zn-N1	2.075(2)	Zn-Cl1	2.2606(7)
Co-N2	2.012(2)	Co-Cl2	2.3219(9)	Zn-N2	2.395(2)	Zn-Cl2	2.2585(8)
Co-N4	2.172(2)			Zn-N4	2.167(3)		
Bond Angles (°)							
N2-Co-Cl2	116.92(7)	N4-Co-Cl1	104.17(8)	N2-Zn-Cl2	90.86(6)	N4-Zn-Cl1	105.01(7)
N2-Co-Cl1	125.42(7)	N4-Co-N2	79.31(10)	N2-Zn-Cl1	94.78(5)	N4-Zn-N2	150.09(9)
Cl1-Co-Cl2	116.58(4)	N1-Co-Cl2	91.21(6)	Cl1-Zn-Cl2	114.65(3)	N1-Zn-Cl2	125.03(6)
N1-Co-N4	153.82(9)	N1-Co-Cl1	94.14(6)	N1-Zn-N4	77.83(10)	N1-Zn-Cl1	118.73(6)
N4-Co-Cl2	97.17(7)	N1-Co-N2	74.81(9)	N4-Zn-Cl2	100.63(7)	N1-Zn-N2	73.00(9)

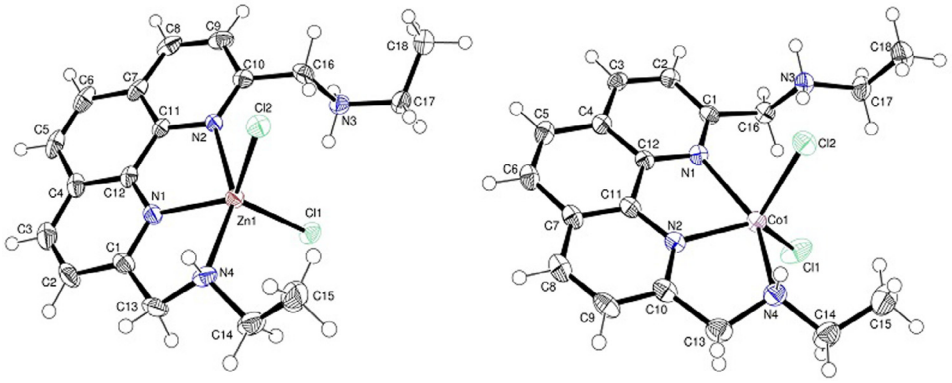

Fig. 2. ORTEP diagram of $[Zn(HL)Cl_2]Cl$ and $[Co(HL)Cl_2]NO_3$ at 50% probability. The anions and water molecules was omitted for clarity (2 column).

configurations (octahedral, square or pyramidal), the possibility of binding L completely is increased.

3.2. Electrochemistry

Redox potentials of the ligands and complexes were obtained by cyclic voltammetry, and they are summarized in Table 3.

Fig. 3 (left) shows the voltammogram obtained for H_3LCl_3 from open circuit potential E_{oc} to a positive direction. One oxidation signal I_a (E_{pa} = 1.124 V), without its corresponding reduction signal was assigned, by the anion exchange test, to an irreversible chloride oxidation ($2Cl^-_{(aq)} = Cl_{2(g)} + 2e^-$). The chloride ion was exchanged for nitrate (NO_3^-) with the stoichiometric amount of AgCl, and new voltammogram (inset Fig. 3 left) was recorded, the result was the disappearance of the signal I_a. When the scan reversed from the inversion potential E_λ to the negative direction, the signal II was detected. The reduction signal II_c, with its corresponding oxidation signal II_a, was associated with ligand reduction. It has been reported that the redox processes of aromatic diimines and those carried out on the aromatic moiety in their complexes are given at negative potential values [50–52]. The signal II is a quasi-reversible process ($E_{1/2}$ = 0.793, ΔE_p = 254 mV and i_{pa}/i_{pc} = 0.76) and according to the signal, shape looks like a coupled electrochemical-chemical process [53]. The shape of the same signal in the anion exchange test suggests that the process becomes reversible (i_{pa}/i_{pc} = 0.97).

Fig. 3 (right) shows the voltammogram, from the open circuit potential to negative potentials, for $[Fe(HL)Cl_2]B\Phi_4$; it was possible to observe four signals. Two subsequent reduction processes of the ligand with their corresponding oxidations ($I_{a,c}$ and $II_{a,c}$); this behavior has been reported previously in complex of Co, Ru and Ni with 1,10-phenanthroline and other aromatic diimines [52]. An oxidation process with its corresponding reduction ($IV_{a,c}$) was detected, and it was assigned, by association with similar Fe(II) complexes [54], to a quasi-reversible iron oxidation. Moreover, an adsorption process (III) was also detected, but the study of these signals is beyond our interest. Analogous redox behavior was found for L in the other coordination compounds, but no oxidation process for the metal ions was observed. The Co(II) shows a reversible redox process Co(III)|Co(II) at 0.226 V vs. Fc^+|Fc, but no oxidation process for the metal ions Mn(II), Ni(II) and Zn(II) was observed. That could be due to their high redox potential values compared with the solvent oxidation under the experimental conditions.

Particularly for $[Cu(L)(H_2O)](NO_3)$, the ligand reduces in one step (E_{pc} = −1.310 V). Two additional electrochemical processes were associated with the transformations of Cu(II)/Cu(I) ($E_{1/2}$ = −0.348 V) and Cu(I)/Cu(0) ($E_{1/2}$ = −0.550 V). Signals were assigned according to reports of similar Cu(II) complex [55,56].

In general, the reduction of L requires more energy in the coordinated state, however, its π-acceptor character and its capacity to participate in back-bonding interactions to redistribute the electron density is evident due to the two subsequent reduction processes on the aromatic moiety of the ligand.

3.3. Theoretical studies

Computational studies were performed to explore the electron density distribution of the ligand, and also in the coordination complexes, The protonation equilibria studies of L suggest that all species, L, HL^+, H_2L^{2+}, and H_3L^{3+}, have similar energy. At pH = 6, employed in the reaction media, the predominant species is H_2L^{2+}, stabilizing this protonated form the hydrogen bonds formed between the nitrogen atoms of the phenanthroline. This experimental result agrees with those reported by Guo and coworkers [22], who informed about the penta-coordination for the Zn(II) derivative. The detailed information regarding the energies and geometries of the most stable species could be consulted in the Supplementary information.

Table 3
Redox potentials for H_3LCl_3 and complexes.

Compound	Ligand	$M^{II}L \rightarrow M^{III}L + e^-$	$M^{II}L + e^- \rightarrow M^{I}L$	$M^{I}L + e^- \rightarrow M^{0} + L$
H_3LCl_3	−0.793	n. o.	n. o.	n. o.
$[Mn(HL)Cl]Cl_2$	−1.341*, −1.942	n. o.	n. o.	n. o.
$[Fe(HL)Cl_2]B(Ph)_4$	−1.055, −1.272	0.442*	n. o.	n. o.
$[Co(HL)Cl_2]Cl$	−1.471, 1.645	0.226	n. o.	n. o.
$[Ni(L)(NO_3)(H_2O)]NO_3$	−1.110*, −1.782	n. o.	n. o.	n. o.
$[Cu(L)(H_2O)](NO_3)_2$	−1.310*	n. o.	−0.348	−0.550
$[Zn(HL)Cl_2]Cl_2$	−1.514, −1.882*	n. o.	n. o.	n. o.

* Quasi-reversible/irreversible process, n. o., not observable. Redox potentials are reported in (V) vs. $Fc^+|Fc$ in 0.1 M de TBAH-DMSO.

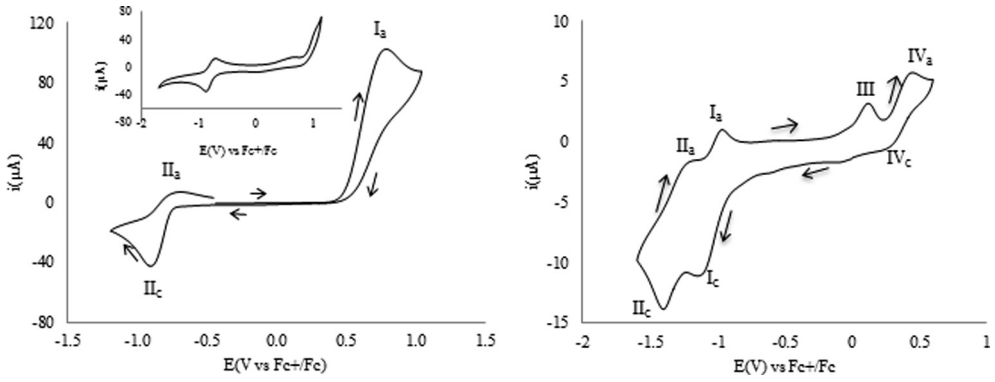

Fig. 3. Cyclic voltammograms of 20 mM H_3LCl_3 (left) and 20 mM of $[Fe(HL)Cl_2)]B(Ph)_4$ in DMSO containing 0.1 M TBAH. The working electrode was Pt. Scan rate 0.1 V/s.

Calculations for the coordination compounds were initialized from the crystallographic structures. Two protonated forms of L (HL^+ and H_2L^{2+}) coordinated to the metal ion were studied. The angular distortion calculated for Co(II) and Zn(II) derivatives is 0.99 and 0.64 respectively. The disagreement with the experimental results could be explained by the fact that the calculations were made in the gas phase, so, the intra and intermolecular interactions were not considered.

The main differences were found at the LUMO orbital energies as the key element to distinguish between two possible states of the ligand (L or HL interacting with the metal ion) and observed in all compounds due to the redox processes. Table 4 shows that HL derivatives present a subtle higher stabilization. Exploration of LUMO orbitals of both systems indicates a similar distribution of the orbitals in the atoms of L. However; the energy behavior is quite different as can be seen in Fig. 4.

As expected, by electrochemical results, the $\Delta_{HOMO\text{-}LUMO}$ value, as well as the energy of the LUMO orbitals of coordination compounds, is highest as the redox potential becomes more negative as observed in Fig. 5 for Mn, Ni, Cu, and Zn. The Fe(II) and Co(II) are outliers, and this could be explained by its capacity to redistribute the electron density. On the other hand, HOMO orbitals of coordination compounds principally involve the metal ion and some atoms of the ligand. The Zn(II) derivative is the main example of electron delocalization in both frontier orbitals, where the participation of the phenanthroline moiety atoms is essential. This result helps to explain why so much energy is needed to electroreduce the ligand.

3.4. Antiproliferative activity

The *in vitro* antiproliferative activity of synthesized compounds was evaluated in HeLa (ATCC) cells after 24 h of drug exposure using the sulforhodamine B (SRB) assay [44,45]. *In vitro* amoebicidal activity was evaluated on cell cultures of *Entamoeba histolytica* trophozoites. The percentage of viable trophozoites was determined with a hematocytometer at three different times: 24, 48 and 72 h using the trypan blue vital exclusion technique·H_2O: DMSO (95:5 v/v) mixture was used to dissolve all compounds. The concentration of DMSO was not toxic neither for tumor cells nor trophozoites. Table 5 show the IC_{50} values. Positive controls: cisplatin and metronidazole (antitumor and amoebicidal drugs respectively) [25] and negative controls with PBS 1X were used.

In HeLa cells, the maximum concentration tested was 300 μM, under these conditions only $[Fe(HL)Cl_2]B(Ph)_4$ exhibited a moderate activity with and IC_{50} = 35.49 μM, that is about five times greater than that of cisplatin (5.5 μM). The activity of this compound, with the lowest redox potential in this work, could be linked to the production of reactive oxygen species (ROS; such as hydroxyl, superoxide and peroxide radicals) associated with cellular damage. On the other hand, although with moderate activity, $[Fe(HL)Cl_2]B(Ph)_4$ contains an essential metal which would make it less toxic to healthy cells and may contribute in the transport of the molecule throughout the cellular environment.

It is important to notice that compound of Fe(II) behaves as an anti-proliferative effector. Meanwhile, coordination compounds (same transition metal ions) with the ligand **L′**: 2,9-bis-(2′,5′-diazahexanyl)-1,10-phenanthroline have been active against the same human tumor cells, being all of them even more potent to inhibit cellular growth than cisplatin, except the Zn derivative [25]. This fact could be associated with the lower stability provided to the compounds by the coordination of L compared with that gained with the coordination of L′. The comparison of the potential redox values (−1.055 and −1.779 V vs. $Fc^+|Fc$) and the antiproliferative activities of Fe(II) coordination compounds at 35.49 μM and 2.4 μM for L and L′, respectively, became evident the influence of the stability of the compounds on their redox behavior and the biological activity.

On the other hand, H_3LCl_3 and the coordination complexes exhibited slight activity against *Entamoeba histolytica* trophozoites cultures. The Co(II) complex (IC_{50} = 162 μM) was the most active, however, is about twenty times lower than the metronidazole

Table 4
Stabilization energies obtained from the calculated coordination compounds involving various protonated forms of L.

Derivative	$[M(L)Cl_2]^+$				$[M(HL)Cl_2]^+$			
	HOMO	LUMO	Δ	Energy kcal/mol	HOMO	LUMO	Δ	Energy kcal/mol
Mn(II)	−0.268	−0.0557	−0.212	−1875.6	−0.3810	−0.169	−0.212	−1875.9
Fe(II)	−0.2649	−0.0519	−0.213	−1946.3	−0.3919	−0.168	−0.224	−1946.6
Co(II)	−0.2717	−0.0541	−0.218	−2021.0	−0.3962	−0.172	−0.224	−2021.3
Ni(II)	−0.2640	−0.0604	−0.204	−2099.8	−0.3889	−0.176	−0.213	−2100.0
Cu(II)	−0.2721	−0.0559	−0.216	−2182.7	−0.4099	−0.170	−0.240	−2183.0
Zn(II)	−0.2729	−0.0557	−0.217	−2269.9	−0.4078	−0.162	−0.246	−2270.1

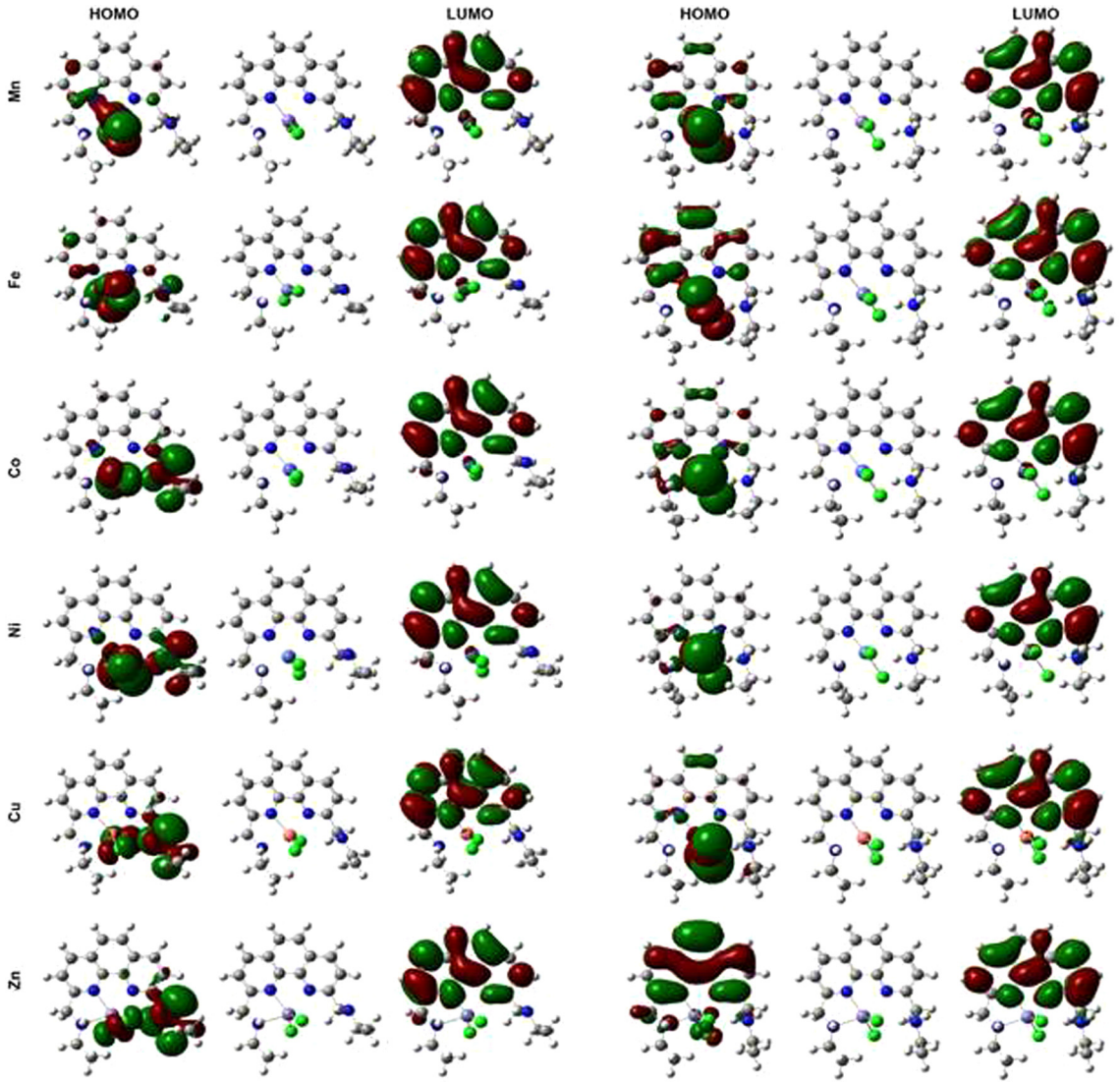

Fig. 4. Grid representations of HOMO and LUMO orbitals for neutral (left) and +1 (right) compounds using an isodensity value of 0.2 a. u.

(6.8 μM). An interesting fact is that the little amoebicidal activity of trihydrochloride ligand increases with the presence of the metal ions, in the case of the Co(II) complex almost thirty times. Su [20], Guo [21,22] and coworkers concluded that polyamine compounds increased the catalytic efficiency when they bound to metals. Similarly, our group demonstrated that antiproliferative activity against trophozoites is due to the coordination compounds instead than the ligand itself [57,58]. In a general way, the antiproliferative activity of the compounds increases as the energy employed for the reduction decreases.

It is notable that the compounds with the highest antiproliferative activity, Fe(II) complex in HeLa cells and Co(II) complex in *E. histolytica*, are the only ones where the metal oxidizes with moderate energy, and those where only L is reduced does not have or present marginal activity. With these results, we can rule out that the ligand reduction is the only process to produce cytotoxicity and that the redox process of the metal ion also contributes in this task [25]. Also, these results suggest that the mechanisms by which these compounds produce cellular damage may be related to an imbalance in the redox system of the cell thus, causing its death.

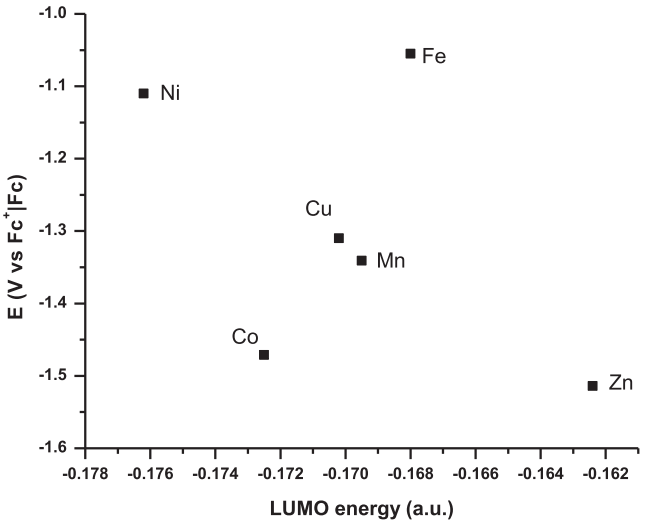

Fig. 5. Redox potential modification as a function of the energy change in the LUMO of coordination compounds. (1 column).

Table 5
Antiproliferative[a] and amoebicide[b] activity (IC_{50}, μM) in human tumor cell lines HeLa and cell cultures of *Entamoeba histolytica* trophozoites of H_3LCl_3 and its coordination compounds.

Compound	IC_{50}(μM)[a] HeLa	IC_{50}(μM)[b] *E. histolityca*
H_3LCl_3	N. A.	4300
$[Mn(HL)Cl]Cl_2$	N. A.	2600
$[Co(HL)Cl_2]NO_3$	N. A.	162
$[Fe(HL)Cl_2]B\Phi_4$	35.49	1300
$[Ni(L)(H_2O)(NO_3)]NO_3$	N. A.	1700
$[Cu(L)(H_2O)](NO_3)_2$	N. A.	3200
$[Zn(HL)Cl_2]Cl$	N. A.	2400
Metronidazole	–	6.8
cis-Pt	5.5	–

N.A.: IC_{50}>300μM.

4. Conclusions

The N4-donor ligand L and its coordination compounds with first-row transition divalent metals Mn(II), Fe(II), Co(II), Ni(II), Cu(II) and Zn(II) were synthesized and fully characterized. Analysis showed that the coordination compounds have different structures, but these almost are the same in the solid state and DMSO solution. In addition, XRD analysis indicated that complexes have a similar pentacoordinate structure for the Co(II) and Zn(II); both are compounds with an intermediate conformation between the ideal geometries, and L acts as a tridentate chelate. Like the geometry, the redox behavior is variable. The ligand in its hydrochloride form can be reduced; the potential of this process becomes more negative when it is bound to a metal ion due to the back-bonding interaction promoted by the π-acceptor capacity of L. Theoretical calculations explain this fact based on the energies found for the LUMO orbitals of the complexes. Calculations also demonstrate that the synthetic conditions determinate the complex configuration. In general, the synthesized compounds had a moderate antitumor and amoebicidal activity. The ligand is active againts *E. histolytica* cultures and the activity is enhanced with the presence of the metal, in some cases thirty times. The most effective compounds are those that present a process of oxidation centered in the metal, this suggests a mechanism of cell damage by redox imbalance. Although the efficacy of these compounds is lower than that observed for traditional drugs, it is necessary to continue studying their properties since the presence of essential metals may produce less toxic and more selective compounds.

Acknowledgment

The authors thank financial support to UNAM from PAIP/FQ 5000-9047, PAPIIT/IG200616, CONACYT for postgraduate students, grant 307725 (LFHA). To Dr. Alberto Vela from Department of Chemistry from CINVESTAV for computing time (SET). To laboratory 9 at the Unidad de Investigación en Diferenciación Celular from the UMIEZ at the FES Zaragoza for cervical cancer cell line donation.

Appendix A. Supplementary data

Supplementary data associated with this article can be found, in the online version, at http://dx.doi.org/10.1016/j.ica.2017.06.040.

References

[1] W. Kaim, B. Schwederski, A. Klein, Bioinorganic Chemistry: Inorganic Elements in the Chemistry of Life An Introduction and Guide, 2nd ed., John Wiley & Sons Ltd, New York, Chichester, 2013.
[2] T.W. Hambley, Science 318 (2007) 1392.
[3] Z. Guo, P.J. Sadler, Agew. Chem. Ed. Engl 38 (1998) 1512.
[4] X. Wang, M. Yan, Q. Wang, H. Wang, Z. Wang, J. Zhao, J. Li, Z. Zhang, Molecules 1 (2017) 22.
[5] L. Ruiz-Azuara, M.E. Bravo-Gómez, Curr. Med. Chem. 17 (2010) 3606.
[6] J. Korbecki, I. Baranowska-Bosiacka, I. Gutowska, D. Chlubek, Postepy Biochem. 62 (2016) 60–65.
[7] P. Jiang, Z. Dong, B. Ma, Z. Ni, H. Duan, X. Li, B. Wang, X. Ma, Q. Wei, X. Ji, M. Li, Appl. Biochem. Biotechnol. 180 (2016) 841.
[8] J.L. Domingo, M. Gómez, Food Chem. Toxicol. 95 (2016) 137.
[9] D. Gambino, Coord. Chem. Rev. 255 (2011) 2193.
[10] F. B. do Nascimento, G. Von Poelhsitz, F. R. Pavan, D. N. Sato, C. Q. F. Leite, H. S. Selistre-de-Araújo, J. Ellena, E. E. Castellano, V. M. Deflon, A. A. Batista, J. Inorg. Biochem., 102 (2008) 1783.
[11] M. Navarro, Coord. Chem. Rev. 253 (2009) 1619.
[12] M.B. Tarallo, C. Urquiola, A. Monge, B. Parajón Costa, R.R. Ribeiro, R.C. Mercader, F.R. Pavan, C.Q.F. Leite, M.H. Torre, D. Gambino, J. Inorg. Biochem. 104 (2010) 1164.
[13] P.G. Sammes, G. Yahioglu, Chem. Soc. Rev. 23 (1994) 327.
[14] K.E. Augustyn, V.C. Pierre, J.K. Barton, *Metallointercalators as probes of DNA recognition and reactions*, in Wiley Encyclopedia of Chemical Biology, vol. 3, 2009, p. 34.
[15] L. Herman, S. Ghosh, E. Defrancq, A. Kirsh-De Mesnaeker, J. Phys. Org. Chem 21 (2008) 670.
[16] R. Galindo-Murillo, J.C. García-Ramos, L. Ruiz-Azuara, T.E. Chaeatham III, F. Cortés-Guzmán, Nucleic Acid Res. 43 (2015) 5364.
[17] Z. Zhang, H. Wang, Q. Wang, M. Yan, H. Wang, C. Bi, S. Sun, Y. Fan, Int. J. Oncol. 49 (2016) 691.
[18] G. Scalese, I. Correia, J. Benítez, S. Rostan, F. Marques, F. Mendes, A.P. Matos, J. Costa-Pesoa, D. Gambino, J. Inorg. Biochem. 166 (2016) 162.
[19] J.C. García-Ramos, A.G. Gutierrez, A. Vázquez-Aguirre, Y. Toledano-Magaña, A. L. Alonso-Sáenz, V. Gómez-Vidales, M. Flores-Álamo, C. Mejía, L. Ruiz-Azuara, Biometals 30 (2017) 43.
[20] X. Su, H. Sun, Z. Zhou, H. Lin, L. Chen, S. Shu, Y. Chen, Polyhedron 20 (2001) 9.
[21] Y. Guo, Q. Ge, H. Lin, S. Shu, C. Zhou, Biophys. Chem. 105 (2003) 119.
[22] Y. Guo, Q. Ge, H. Lin, H. Lin, S. Zhu, C. Zhou, J. Mol. Recognit 16 (2003) 102.
[23] Z. Wang, H. Lin, Z. Zhou, M. Xu, T. Liu, S. Zhu, Y. Chen, Bioorg. Med. Chem. 9 (2001) 2849.
[24] G. Zhao, H. Sun, H. Lin, S. Zhu, X. Su y, Y. Shen, J. Inorg. Biochem. 72 (1998) 173.
[25] J.C. García-Ramos, Y.T. Magaña, L.G. Talavera-Contreras, M. Flores-Álamo, V. Ramírez-Delgado, E. Morales-León, L.A. Ortíz-Frade, A.G. Gutíerrez, A. Vázquez Aguirre, C. Mejía, J.C. Carrero, J.P. Laclette, R. Moreno-Esparza y, L. Ruiz-Azuara, Dalton Trans. 41 (2012) 10164.
[26] S.A. Abushameh, H.A. Goodwin, Aust. J. Chem. 33 (1980) 2171.
[27] X.C.H. Chandler, L.W. Deady, J.A. Reiss, J. Heterocycl. Chem. 18 (1981) 599.
[28] D. Laventine, A. Afsar, M.J. Hudson, L.M. Harwood, Heterocycles 86 (2) (2012) 1419–1429.
[29] G. Gritzner, J. Küta., Pure Appl. Chem., 4 (1984) 461.
[30] Agilent, CrysAlis PRO and CrysAlis RED, Agilent Technologies, Yarnton, England, 2013.
[31] R.C. Clark, J.S. Reid, Acta Cryst. Sect. A 51 (1995) 887.
[32] G.M. Sheldrick, Acta Cryst. A71 (2015) 3.
[33] L.J. Farrugia, J. Appl. Crystallogr. 30 (1997) 565.
[34] L.J. Farrugia, J. Appl. Crystallogr. 32 (1999) 837.
[35] M. J. Frisch, G. W. Trucks, H. B. Schlegel, G. E. Scuseria, M. A. Robb, J. R. Cheeseman, J. A. Montgomery, T. Vreven, K. N. Kudin, J. C. Burant, Gaussian 09, Revision D.01. Gaussian Inc. 2009.

[36] E.G. Hohenstein, S.T. Chill, C.D. Sherrill, J. Chem. Theory Comput. 4 (12) (2008) 1996.
[37] Y. Zhao, D.G. Truhlar, Theor. Chem. Acc. 120 (2007) 215.
[38] A.M. Köster, A.P. Calaminici, M.E. Casida, V.D. Domínguez-Soria, R. Flores-Moreno, G. Geudtner, A. Goursot, T. Heine, A. Ipatov, F. Janetzko, J. Martin delCampo, S. Patchkovskii, J.U. Reveles, D.R. Salahub, A. Vela, deMon2k, (Version3). The DeMon Developers, Cinvestav, Mexico City, 2011.
[39] N. Godbout, D.R. Salahub, J. Andzelm, E. Wimmer, Can. J. Chem. 70 (1992) 560.
[40] P. Perdew, K. Burke, M. Ernzerhof, Phys. Rev. Lett. 77 (1996) 3865.
[41] R. Galindo-Murillo, T.E. Cheatham III, Chem. Med. Chem. 9 (2014) 1252.
[42] J.C. García-Ramos, R. Galindo-Murillo, F. Cortés-Guzmán, L. Ruiz-Azuara, J. Mex. Chem. Soc. 57 (2013) 245.
[43] J.C. García-Ramos, G. Vértiz-Serrano, L. Macías-Rosales, R. Galindo-Murillo, Y. Toledano-Magaña, J.P. Bernal, F. Cortés-Guzmán, L. Ruiz-Azuara, Eur. J. Inorg. Chem. (2017), http://dx.doi.org/10.1002/ejic.201601199.
[44] L.V. Rubinstein, R.H. Shoemaker, K.D. Paull, R.M. Simon, S. Tosini, P. Skehan, D. A. Scudiero, A. Monks, M.R. Boyd, J. Natl. Cancer Inst. 82 (1990) 1113.
[45] P. Skehan, R. Storeng, D. Scudiero, A. Monks, J. McMahon, D. Vistica, J.T. Warren, H. Bokesch, S. Kenney, M.R. Boyd, J. Natl. Cancer Inst. 82 (1990) 1107.
[46] H. Sun, H. Lin, Z. Zhou, G. Zhao, X. Su, S. Zhu y, Y. Chen, Indian J. Chem. 40A (2001) 763.
[47] Y. Vargas-Rodríguez, V. Gómez-Vidales, E. Vázquez-Labastida, A. García-Borquez, G. Aguilar-Sahagún, H. Murrieta-Sánchez, M. Salmon, Rev. Mex. Cienc. Geol. 25 (2008) 135.
[48] K. Nakamoto, Infrared and Raman Spectra of Inorganic Compounds, 5th ed., John Wiley and Sons, Michigan, 1997.
[49] B.J. Hathaway, D.E. Billing, Coord. Chem. Rev. 5 (1970) 143.
[50] A. Juris, V. Balzani, F. Barigelletti, S. Campagna, P. Belser, A. von Zelewsky, Coord. Chem. Rev. 84 (1988) 85.
[51] L.A. Ortiz-Frade, L. Ruiz-Ramírez, I. González, A. Marín-Becerra, M. Alcarazo, J. G. Alvarado-Rodríguez y, R. Moreno-Esparza, Inorg. Chem. 42 (2003) 1825–1834.
[52] S. Arounaguiri, D. Easwaramoorthy, A. Ashokkumar, A. Dattagupta, B. Maiya, Proc. Indian Acad. Sci. (Chem. Sci.), 112 (2000) 1.
[53] G.A. Mabbott, J. Chem. Educ. 60 (1983) 697.
[54] H.M. Naseem-Akhtar, A.A. Shaikh, M.Q. Eshan, Rus. J. Electrochem 44 (2008) 1403.
[55] M. Manzanera-Estrada, L.F. Hernández Ayala, G. Osorio-Monreal, J.C. García-Ramos, L.A. Ortíz-Frade, J. Mex. Chem. Soc. 57 (2013) 192.
[56] D. Rodríguez-Torres, J.C. García-Ramos, J. Manríquez, R. Moreno-Esparza, M. Altamirano-Lozano, I. González, J. Gracia-Mora, L. Ruiz-Azuara, R. Antaño-López, L.A. Ortiz-Frade, Polyhedron 28 (2009) 1186.
[57] C. Sarniguet, J. Toloza, M. Cipriani, M. Lapier, M. Vieites, Y. Toledano-Magaña, J. C. García-Ramos, L. Ruiz-Azuara, V. Moreno, J.D. Maya, C. Olea-Azar, D. Gambino, L. Otero, Biol. Trace Elem. Res. 159 (2014) 379.
[58] Y. Toledano-Magaña, J.C. García-Ramos, C. Torres-Gutiérrez, C. Vázquez-Gasser, J.M. Esquivel-Sánchez, M. Flores-Alamo, L. Ortiz-Frade, R. Galindo-Murillo, J.P. Laclette, J.C. Carrero, Lena. Ruiz-Azuara, Med. Chem. 60 (2017) 899.